Fluorescence from atmospheric aerosols observed with a multi-channel lidar spectrometer

Nobuo Sugimoto,[1,*] Zhongwei Huang,[2] Tomoaki Nishizawa,[1] Ichiro Matsui,[1] and Boyan Tatarov[3]

[1]*National Institute for Environmental Studies, 16-2 Onogawa, Tsukuba, Ibaraki 305-8506, Japan*
[2]*College of Atmospheric Sciences, Lanzhou University, Lanzhou, 730000, China*
[3]*Atmospheric Remote Sensing Laboratory, Gwangju Institute of Science and Technology, Oryong-dong, Buk-Gu, Gwangju 500-712, South Korea*
[*]*nsugimot@nies.go.jp*

Abstract: A lidar for measuring fluorescence from atmospheric aerosols was constructed with a third harmonic Nd:YAG laser, a 1-m diameter telescope, and a 32-channel time-resolved photon-counting spectrometer system. Fluorescence spectrum and vertical distribution of fluorescent aerosols in the lower atmosphere were observed during the nighttime with excitation at 355 nm. Relatively strong broad fluorescence was observed from Asian dust and air-pollution aerosols transported from urban and industrial areas. Rough estimates of the fluorescence efficiency were given for these aerosols. The intensity of the total fluorescence over the spectral range from 420 to 510 nm was comparable to that of nitrogen vibrational Raman scattering. That indicates the possibility of making a compact Raman-Mie-fluorescence lidar for aerosol monitoring.

OCIS codes: (280.3640) Lidar; (010.1110) Aerosols; (300.2530) Fluorescence, laser-induced.

References and links

1. T. Maki, S. Susuki, F. Kobayashi, M. Kakikawa, Y. Tobo, M. Yamada, T. Higashi, A. Matsuki, C. Hong, H. Hasegawa, and Y. Iwasaka, "Phylogenetic analysis of atmospheric halotolerant bacterial communities at high altitude in an Asian dust (KOSA) arrival region, Suzu City," Sci. Total Environ. **408**(20), 4556–4562 (2010).
2. F. Kobayashi, S. Morosawa, T. Maki, M. Kakikawa, M. Yamada, Y. Tobo, C.-S. Hon, S. Matsuki, and Y. Iwasaka, "Atmospheric bioaerosol, bacillus sp., at an altitude of 3,500 m over the Noto Peninsula: Direct sampling via aircraft," Asian J. Atmos. Environ. **5**(3), 164–171 (2011).
3. S. C. Hill, R. G. Pinnick, S. Niles, Y.-L. Pan, S. Holler, R. K. Chang, J. Bottiger, B. T. Chen, C.-S. Orr, and G. Feather, "Real-time measurement of fluorescence spectra from single airborne biological particles," Field Anal. Chem. Technol. **3**(4–5), 221–239 (1999).
4. V. Sivaprakasam, A. L. Huston, C. Scotto, and J. D. Eversole, "Multiple UV wavelength excitation and fluorescence of bioaerosols," Opt. Express **12**(19), 4457–4466 (2004).
5. A. Manninen, M. Putkiranta, J. Saarela, A. Rostedt, T. Sorvajärvi, J. Toivonen, M. Marjamäki, J. Keskinen, and R. Hernberg, "Fluorescence cross sections of bioaerosols and suspended biological agents," Appl. Opt. **48**(22), 4320–4328 (2009).
6. Y.-L. Pan, S. C. Hill, R. G. Pinnick, J. M. House, R. C. Flagan, and R. K. Chang, "Dual-excitation-wavelength fluorescence spectra and elastic scattering for differentiation of single airborne pollen and fungal particles," Atmos. Environ. **45**(8), 1555–1563 (2011).
7. V. Sivaprakasam, H.-B. Lin, A. L. Huston, and J. D. Eversole, "Spectral characterization of biological aerosol particles using two-wavelength excited laser-induced fluorescence and elastic scattering measurements," Opt. Express **19**(7), 6191–6208 (2011).
8. C. Pöhlker, J. A. Huffman, and U. Poschl, "Autofluorescence of atmospheric bioaerosols - fluorescent biomolecules and potential interferences," Atmos. Meas. Tech. **5**(1), 37–71 (2012).
9. S. Veerabuthiran and A. K. Razdan, "Parametric studies of fluorescence LIDAR for detection of biological warfare agents in the atmosphere," J. Battlefield Tech. **14**, 5–12 (2011).
10. F. Immler, D. Engelbart, and O. Schrems, "Fluorescence from atmospheric aerosol detected by a lidar indicates biogenic particles in the lowermost stratosphere," Atmos. Chem. Phys. **5**(2), 345–355 (2005).
11. B. Tatarov, N. Sugimoto, I. Matsui, D.-H. Shin, and D. Müller, Multi-channel lidar spectrometer for atmospheric aerosol typing on the basis of chemical signature in Raman spectra, Proc. 25th Int. Laser Radar Conf. 47–50 (2010).

#172038 - $15.00 USD Received 6 Jul 2012; revised 22 Aug 2012; accepted 23 Aug 2012; published 27 Aug 2012

12. B. Tatarov, D. Müller, D. H. Shin, S. K. Shin, I. Mattis, P. Seifert, Y. M. Noh, Y. J. Kim, and N. Sugimoto, "Lidar measurements of Raman scattering at ultraviolet wavelength from mineral dust over East Asia," Opt. Express **19**(2), 1569–1581 (2011).
13. A. Shimizu, N. Sugimoto, I. Matsui, K. Arao, I. Uno, T. Murayama, N. Kagawa, K. Aoki, A. Uchiyama, and A. Yamazaki, "Continuous observations of Asian dust and other aerosols by polarization lidar in China and Japan during ACE-Asia," J. Geophys. Res. **109**(D19), D19S17 (2004).
14. N. Sugimoto, I. Matsui, A. Shimizu, T. Nishizawa, Y. Hara, C. Xie, I. Uno, K. Yumimoto, Z. Wang, and S.-C. Yoon, "Lidar Network Observations of Tropospheric Aerosols," Proc. SPIE **7153**, 71530A, 71530A-13 (2008).
15 A. Shimizu, N. Sugimoto, I. Matsui, I. Mori, M. Nishikawa, and M. Kido, "Relationship between lidar-derived dust extinction coefficients and mass concentrations in Japan," in Scientific Online Letters on the Atmosphere **7A**, 1–4 (2011), doi: http://dx.doi.org/10.2151/sola.7A-001.
16. H. Inaba, "Detection of atoms and molecules by Raman and resonance fluorescence," in *Laser Monitoring of the Atmosphere* (Springer-Verlag, 1976).
17. O. Dubovik, B. Holben, T. F. Eck, A. Smirnov, Y. J. Kaufman, M. D. King, D. Tanre, and I. Slutsker, "Variability of absorption and optical properties of key aerosol types observed in worldwide locations," J. Atmos. Sci. **59**(3), 590–608 (2002).
18. D. Müller, U. Wandinger, D. Althausen, and M. Fiebig, "Comprehensive particle characterization from three-wavelength Raman-lidar observations: case study," Appl. Opt. **40**(27), 4863–4869 (2001).

1. Introduction

A large fraction of atmospheric aerosols is of biological origin. This includes pollen, spore, bacilli, viruses, and biogenic organic materials. A recent study indicated that bacilli are often found on transported Asian dust particles [1, 2]. One of our original motivations of the present study was to detect bacilli on Asian dust particles using fluorescence. Detection of bioaerosols using fluorescence has been studied by a number of researchers [3–7]. Recently, Pöhlker et al. published a comprehensive study of the excitation-emission matrices of atmospheric bioaerosols and interfering materials [8]. The results suggested the possibility of categorizing bio-materials using two excitation wavelengths.

Lidars for measuring fluorescence from aerosols have also been studied by several researchers. Some of them are used for detecting biological weapons [9]. As for atmospheric aerosols, Immler et al. reported a strong signal in the water-vapor Raman channel, and they attributed the signal to fluorescence from forest-fire smoke [10].

We have constructed a lidar spectrometer using a Nd:YAG laser, a 1-m diameter telescope, and a spectrograph with a 32-channel multi-anode photomultiplier tube. The 32-channel multi-spectral lidar detector was originally introduced into our high-spectral-resolution lidar system for studying Raman scattering of SiO_2 in Asian dust [11, 12]. In this paper, we present the results of our initial experiments on the measurement of fluorescence from atmospheric aerosols using the lidar spectrometer. We used a single excitation wavelength of 355 nm and recorded fluorescence spectra in the spectral range from 420 to 510 nm. The present study aims at determining the climatology of fluorescent aerosols in the lower atmosphere.

2. Experiments

Figure 1 presents the configuration of the lidar spectrometer. It employs a third-harmonic Nd:YAG laser, a 1-m diameter telescope, and a 32-channel multi-spectral lidar detector (Licel). The lidar also detects the Mie-scattering signal and the depolarization ratio. The typical output of the laser was 100 mJ at 355 nm, and the laser repetition rate was 30 Hz. The telescope is Newtonian with a focal length of 4048 mm. The field of view of the receiving system was 0.25 mrad. The 32-channel multi-spectral lidar detector consists of a F/3.7 crossed Czerny-Turner spectrograph with 125-mm focal length (Oriel MS125-77400) and a 32-channel photon-counting system using a multi-anode photomultiplier (Hamamatsu H7260-20). A grating with 1200 lines/mm was used, and the spectrum of the backscattered light was recorded in the spectral range from 345 nm to 525 nm with a 5.8-nm resolution over a height range up to 15,000 m with a 15-m height resolution. The slit width at the entrance of the spectrograph was 0.8 mm. A long-pass filter with a cutoff wavelength of 360 nm was used before the spectrograph. The transmission at the laser wavelength was less than 10^{-6} with the

#172038 - $15.00 USD Received 6 Jul 2012; revised 22 Aug 2012; accepted 23 Aug 2012; published 27 Aug 2012

filter and the dichroic mirror in front. The measurement was limited to the nighttime because of the solar background radiation.

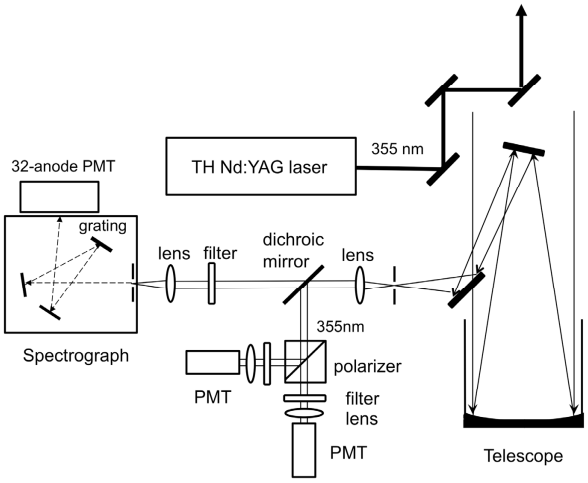

Fig. 1. Configuration of the lidar spectrometer system.

The experiments were performed at the National Institute for Environmental Studies in Tsukuba, Japan (140.12E, 36.05N). To date, nineteen cases including three Asian dust events were observed. We report results of typical cases in this paper. In the data analysis, we also used data from the compact lidar operated continuously at NIES in the Asian Dust lidar network (AD-Net). The lidar is a dual-wavelength lidar (532 nm, 1064 nm) with a polarization receiver (532 nm) and a nitrogen Raman detector (608 nm) [13, 14].

The lidar spectrometer signals were accumulated for 10 minutes and recorded. First, the sensitivity of the multi-channel detector was calibrated. The background signal in each detection channel was estimated from the averaged signal from 6,000 to 15,000 m where the intensity of the lidar return was sufficiently low, and the background was subtracted from the signal. The signal intensity of the spectral channel at each height was normalized by the intensity of the nitrogen Raman scattering channel. This procedure approximately canceled the effect of the geometrical form factor. The effect of attenuation of the transmitted laser was also canceled. The difference in attenuation in the return path due to the difference in wavelength remains but can be neglected in the lower heights where the attenuation itself is small. The fluorescence intensity profiles were further corrected by the molecular density profile so that the intensity at each height was relative to nitrogen Raman scattering at standard ambient temperature and pressure.

We studied the distribution of fluorescent aerosols using the time-height indications of the total fluorescence integrated from 420 to 510 nm. We compared the distribution of fluorescent aerosols with that of non-spherical (dust) and spherical (air pollution) aerosols derived with the AD-Net lidar and identified the aerosol types. We then studied the difference in the fluorescence spectra for dust and air-pollution aerosols. Also, we studied the fluorescence efficiency of these aerosols for several cases. In the analysis of the AD-Net lidar, we first applied the Fernald's method with a constant lidar ratio (S_1 = 50 sr) to derive the extinction coefficient, and then we estimated the mixing ratio of non-spherical and spherical aerosols using the particle depolarization ratio, based on an assumption of external mixing of the two types of aerosols having different particle depolarization ratio. The details of the method are described in references [13, 15]. A similar analysis is possible with the 355-nm data of the lidar spectrometer. However, we used the data of the AD-Net lidar in this paper because the particle depolarization ratio of Asian dust at 355 nm is not well characterized at present.

#172038 - $15.00 USD Received 6 Jul 2012; revised 22 Aug 2012; accepted 23 Aug 2012; published 27 Aug 2012

3. Results and discussion

Figure 2 plots examples of fluorescence spectra for different aerosol and cloud cases. The spectra are normalized by the intensity of nitrogen Raman scattering. The spectra were broad, and no significant structures were observed. However, the shape of the spectrum differed slightly for Asian dust and air-pollution aerosols. The intensity at long wavelengths was higher in the Asian dust than in the air-pollution aerosols. Some of the clouds (but not all) exhibited strong fluorescence. The spectra from the clouds differed from those from the aerosols.

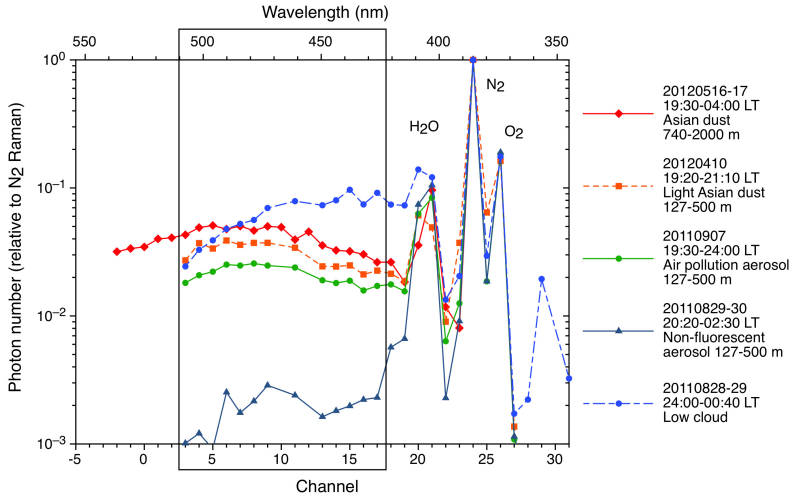

Fig. 2. Examples of the measured fluorescence spectra for aerosol and clouds. The detector sensitivity was corrected. The rectangular area defines the broadband fluorescence used in the fluorescent aerosol profile analysis. (The grating angle setting was different for May 16-17, 2012, and the channel number is shifted.)

We define the intensity (photon number) of the broad fluorescence by integrating the spectra from 420 nm to 510 nm. Figure 3 presents profiles of the fluorescence of the aerosols and cloud. Figure 3 presents the fluorescence intensity relative to nitrogen Raman scattering at standard ambient temperature and pressure. The error bars represent the standard deviations. The error due to background radiation was high even in the nighttime because of the wide spectral bandwidth in the fluorescence measurement. It can be seen in Fig. 3 that Asian dust exhibited strong fluorescence. The fluorescence intensity should depend on the aerosol density and the fluorescence efficiency. We present rough estimates of the fluorescence efficiency in the following.

Figures 4 to 6 present time-height indications of the broad fluorescence in the 420 to 510 nm range for the three cases. The center and right panels in the figures indicate the dust (non-spherical) extinction coefficient and the spherical (mostly air pollution) aerosol extinction coefficients at 532 nm derived from the AD-Net lidar operated at NIES.

In Fig. 4(b), Asian dust was observed at heights above 750 m. The distribution pattern of the fluorescence is similar to that of Asian dust, and the intensity is high. A similar structure is also seen in spherical aerosol above 750 m, indicating a mixing state of dust and air-pollution aerosols. However, the distribution pattern seen in air-pollution aerosol below 750 m is not seen in the fluorescence intensity distribution except for the portion indicated by circle B. This indicates that most of the fluorescence was emitted from Asian-dust particles.

#172038 - $15.00 USD Received 6 Jul 2012; revised 22 Aug 2012; accepted 23 Aug 2012; published 27 Aug 2012

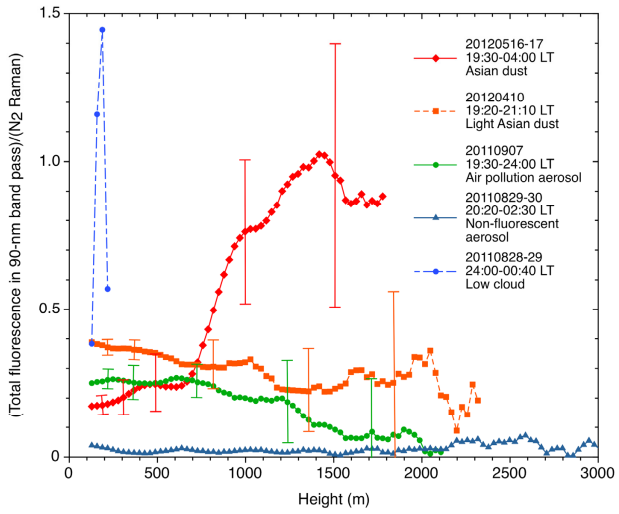

Fig. 3. Profiles of normalized total fluorescence (420 to 510 nm) for Asian dust, air-pollution aerosol, non-fluorescent aerosol, and low clouds.

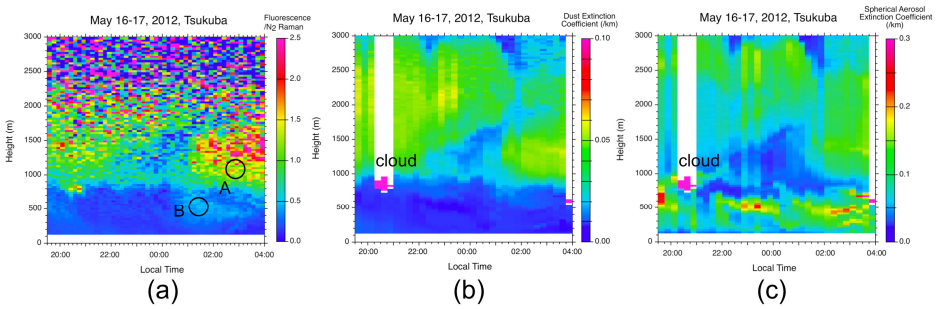

Fig. 4. Time-height indications of (a) broad fluorescence, (b) the non-spherical aerosol extinction coefficient at 532 nm, and (c) the spherical aerosol extinction coefficient at 532 nm for Asian dust case on May 16-17, 2012. Clouds are indicated in magenta, and the areas where no data are available (e.g. above clouds) are indicated in white.

Figure 5 depicts the air-pollution aerosol case. The dust extinction coefficient was low, and no Asian-dust transport was reported. The distribution pattern of the fluorescence is similar to the spherical aerosol extinction coefficient in this case.

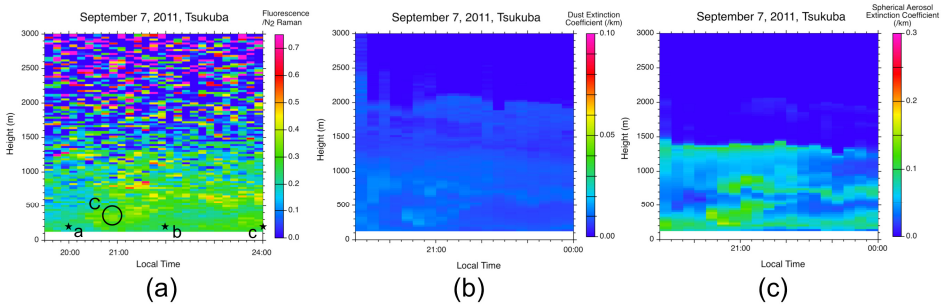

Fig. 5. The same as Fig. 4, but for air-pollution aerosol on September 7, 2011.

#172038 - $15.00 USD Received 6 Jul 2012; revised 22 Aug 2012; accepted 23 Aug 2012; published 27 Aug 2012

Figure 6 also presents an air-pollution aerosol case, but the fluorescence exhibits an interesting structure in the lower heights, where there are low-fluorescence-intensity areas. The distribution pattern of spherical aerosol in the right panel is complicated and no simple correlation is seen.

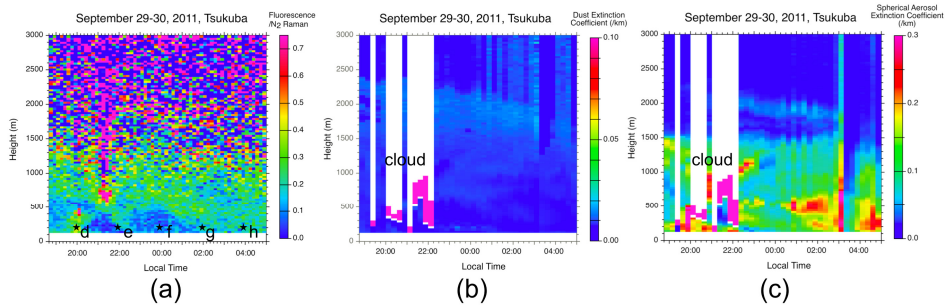

Fig. 6. The same as Fig. 4, but for air-pollution aerosol on September 29-30, 2011.

We performed a trajectory analysis using the NOAA Hybrid Single Particle Lagrangian Integrated Trajectory Model (HYSPLIT) to understand the difference between fluorescent and non-fluorescent aerosols. (http://ready.arl.noaa.gov/HYSPLIT.php) Fig. 7 presents the results for the cases in Figs. 5 and 6. Tsukuba is located about 50 km northeast of Tokyo. The result of the back trajectory analysis indicated that air masses transported over urban and industrial areas in Tokyo, Yokohama, and Chiba often exhibited fluorescence. In the September 7 case, the trajectories ending at a, b, and c are all from the industrial area. In the September 29 case, the trajectories ending at g and h pass over Tokyo, but d, e, and f pass over the north of Tokyo. The fluorescence intensity at f was low in Fig. 6. The fluorescence intensities at d and e were not low, but this was probably due to the clouds seen in Fig. 6. The trajectories ending at a 1000-m height in Fig. 6 all pass over industrial areas (not shown).

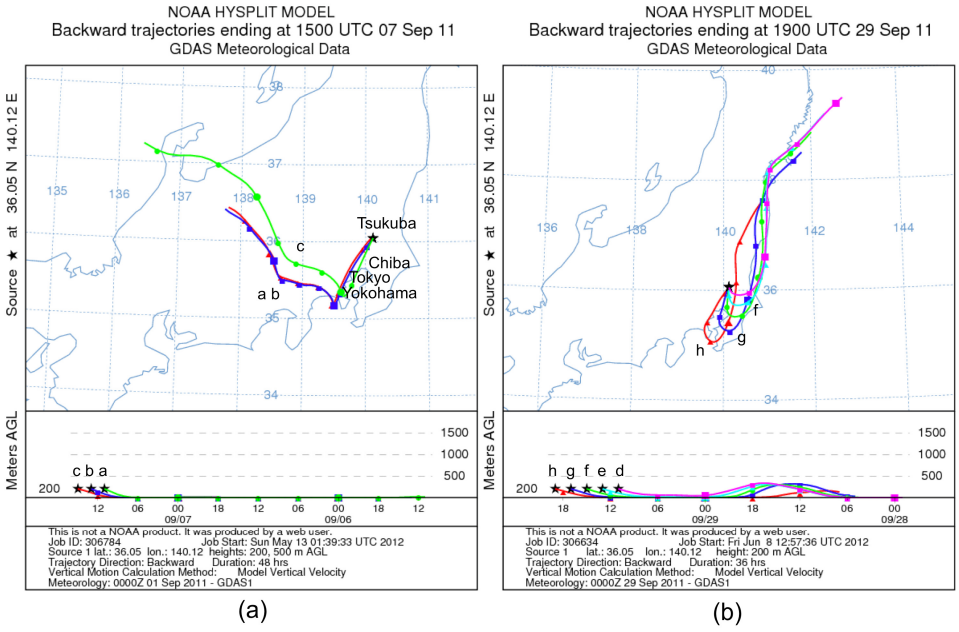

Fig. 7. Back trajectories for (a) September 7, 2011, and (b) September 29, 2011.

#172038 - $15.00 USD Received 6 Jul 2012; revised 22 Aug 2012; accepted 23 Aug 2012; published 27 Aug 2012

The fluorescence intensity depends on the aerosol concentration and the fluorescence efficiency. We may write the relationship between the backward fluorescence coefficient and the aerosol backscattering coefficient as follows.

$$\beta_{fl} = \eta_{fl} \cdot \frac{(1-SSA)}{SSA} f \cdot \beta_{Mie} := C_{fl} \cdot \beta_{Mie} . \quad (1)$$

Here, β_{fl} is the backward fluorescence coefficient ($m^{-1}sr^{-1}$), β_{Mie} is the backscattering coefficient ($m^{-1}sr^{-1}$), *SSA* is the aerosol single-scattering albedo, and η_{fl} is the fluorescence efficiency. The factor *f* represents the difference between the Mie scattering phase function and that for fluorescence. We may call the coefficient C_{fl} the "lidar fluorescence ratio," though it depends on the spectral bandwidth of the fluorescence measurement. β_{fl} can be estimated from the measurements because the fluorescence intensity is scaled with nitrogen Raman scattering. The total vibrational Raman scattering coefficient of nitrogen at standard ambient temperature and pressure (25deg C, 1 bar) is $6.80 \cdot 10^{-9}$ $m^{-1}sr^{-1}$ at 355 nm [16].

The backward fluorescence coefficient β_{fl} for the total fluorescence in the 90-nm bandwidth is $1.5 \cdot 10^{-8}$ $m^{-1}sr^{-1}$ for the Asian-dust case in Fig. 4, marked with "A." The dust backscatter coefficient at 355 nm is $1.0 \cdot 10^{-6}$ $m^{-1}sr^{-1}$. The coefficient C_{fl} in Eq. (1) is $1.5 \cdot 10^{-2}$. *SSA* for Asian dust at 355 nm is about 0.9 [17], if we suppose $f \sim 1$, η_{fl} is estimated to be 0.15. If we do the same thing for the spherical aerosol in Fig. 5, marked "C," β_{fl} $\sim 2.1 \cdot 10^{-9}$ $m^{-1}sr^{-1}$, $\beta_{Mie,355}$ $\sim 3 \cdot 10^{-6}$ $m^{-1}sr^{-1}$, and C_{fl} $\sim 7 \cdot 10^{-4}$. *SSA* for air-pollution aerosols varies depending on the aerosol type. If we suppose *SSA* to range from 0.9 to 0.99 and $f \sim 1$, we obtain η_{fl} ~0.007-0.07. In the same way, we estimated C_{fl} $\sim 1.1 \cdot 10^{-3}$ for the non-dust aerosol in Fig. 4, marked with "B," C_{fl} $\sim 7 \cdot 10^{-5}$ for the non-fluorescent aerosol in Fig. 3, and C_{fl} $\sim 2.4 \cdot 10^{-4}$ for the fluorescent cloud in Fig. 3. Table 1 summarizes the estimated C_{fl} and η_{fl}. Please note that these are very rough estimates for very limited cases. The *SSA* values are not derived but are just assumed. Also factor *f* in Eq. (1) was assumed to be 1.

Table 1. Rough estimate of the lidar fluorescence ratio C_{fl} and the fluorescence efficiency η_{fl} for the aerosol and cloud cases observed in this study

Target	β_{fl}($m^{-1}sr^{-1}$)	β_{Mie}($m^{-1}sr^{-1}$)	C_{fl}	*SSA* (assumption)	η_{fl}
Asian dust (Fig. 4 "A")	$1.5\ 10^{-8}$	$1.0\ 10^{-6}$	$1.5\ 10^{-2}$	0.9	0.15
Non-dust aerosol (Fig. 4 "B")	$5\ 10^{-9}$	$4.5\ 10^{-6}$	$1.1\ 10^{-3}$	0.9-0.99	0.01-0.1
Air-pollution aerosol (Fig. 5 "C")	$2.1\ 10^{-9}$	$3\ 10^{-6}$	$7\ 10^{-4}$	0.9-0.99	0.007-0.07
Non-fluorescent aerosol (Fig. 3)	$5\ 10^{-10}$	$7.5\ 10^{-6}$	$7\ 10^{-5}$	0.9-0.99	0.0007-0.007
Fluorescent cloud (Fig. 3)	$1.2\ 10^{-8}$	$5\ 10^{-5}$	$2.4\ 10^{-4}$	0.99	0.024

The result indicates that Asian dust is highly fluorescent. We suppose that the fluorescence of Asian dust is mostly from the mineral material itself, though there may be other materials attached to the dust surface. We are planning a laboratory experiment using Asian-dust samples. The fluorescence efficiency of spherical aerosols is highly variable. The fluorescence intensity of clouds was high in Fig. 3, but the fluorescence efficiency was not very high. The number of the cases we have observed (currently 19) is still not sufficient. We

#172038 - $15.00 USD Received 6 Jul 2012; revised 22 Aug 2012; accepted 23 Aug 2012; published 27 Aug 2012

have not observed, for example, biomass-burning smoke, which is expected to be highly fluorescent. Also, we have not observed pure dust cases. In this paper, we have presented only a rough estimate of the fluorescence efficiency, based on assumptions about *SSA* and the scattering-phase function factor. The fluorescence efficiency should be analyzed based on aerosol microphysical properties obtained from multi-wavelength Raman or high-spectral resolution lidars [18]. The fluorescence efficiency would provide additional information for characterizing aerosols.

The intensity of the broad fluorescence of fluorescent aerosols was comparable to the nitrogen vibrational Raman scattering intensity as can be seen in Fig. 2 and Fig. 3. This suggests the possibility of creating a compact fluorescence lidar with two or three broadband detection channels. Some categorization of aerosols would be possible using the difference in the spectral shape of the fluorescence between mineral dust and air-pollution aerosols. To obtain fundamental data for such applications, we plan to extend the spectral range of the lidar spectrometer to longer wavelengths.

4. Conclusion

We constructed a multi-channel lidar spectrometer and studied fluorescence of atmospheric aerosols with excitation at 355 nm. We studied distribution of fluorescent aerosols, fluorescence spectrum, and the fluorescence efficiency. The results showed that Asian dust and some of air-pollution aerosols transported from the urban and industrial areas are fluorescent. The results suggest the fluorescence measurement provides useful information for aerosol characterization when it is performed simultaneously with the measurement of microphysical parameters of aerosols by a multi-wavelength Raman lidar or high-spectral-resolution lidar. We plan to continue the observation with the lidar spectrometer to study characteristics of fluorescent aerosols, and we also plan to refine the analysis method using the Raman scattering data from the lidar spectrometer and the AD-Net lidar for estimating the fluorescence efficiency more quantitatively.

#172038 - $15.00 USD Received 6 Jul 2012; revised 22 Aug 2012; accepted 23 Aug 2012; published 27 Aug 2012